Journal of Applied Physics

The impact of cathode surface roughness and multiple breakdown events on microscale gas breakdown at atmospheric pressure

Cite as: J. Appl. Phys. **125**, 203302 (2019); https://doi.org/10.1063/1.5085217
Submitted: 10 December 2018 . Accepted: 30 April 2019 . Published Online: 24 May 2019

Russell S. Brayfield, Andrew J. Fairbanks, Amanda M. Loveless, Shengjie Gao, Agni Dhanabal, Weihang Li, Caleb Darr, Wenzhuo Wu, and Allen L. Garner

View Online Export Citation CrossMark

ARTICLES YOU MAY BE INTERESTED IN

Unification of field emission and space charge limited emission with collisions
Applied Physics Letters **114**, 014103 (2019); https://doi.org/10.1063/1.5066236

Change in chemical bonding state by thermal treatment in MgO-based magnetic tunnel junction observed by angle-resolved hard X-ray photoelectron spectroscopy
Journal of Applied Physics **125**, 203903 (2019); https://doi.org/10.1063/1.5094067

A universal theory for gas breakdown from microscale to the classical Paschen law
Physics of Plasmas **24**, 113522 (2017); https://doi.org/10.1063/1.5004654

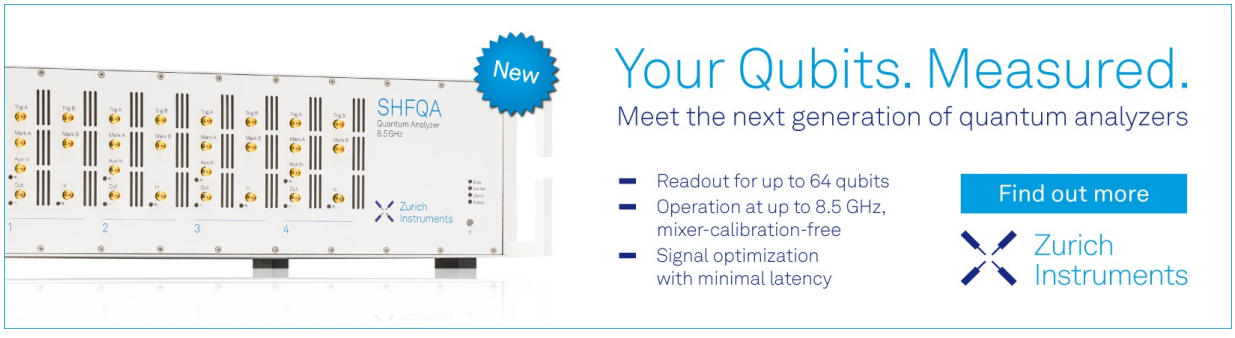

© 2019 Author(s).

Journal of Applied Physics ARTICLE scitation.org/journal/jap

The impact of cathode surface roughness and multiple breakdown events on microscale gas breakdown at atmospheric pressure

Cite as: J. Appl. Phys. **125**, 203302 (2019); doi: 10.1063/1.5085217
Submitted: 10 December 2018 · Accepted: 30 April 2019 ·
Published Online: 24 May 2019

View Online Export Citation CrossMark

Russell S. Brayfield II,[1] Andrew J. Fairbanks,[2] Amanda M. Loveless,[2] Shengjie Gao,[3] Agni Dhanabal,[4] Weihang Li,[1] Caleb Darr,[2] Wenzhuo Wu,[3] and Allen L. Garner[2,4,5,a)]

AFFILIATIONS

[1]School of Aeronautics and Astronautics, Purdue University, West Lafayette, Indiana 47907, USA
[2]School of Nuclear Engineering, Purdue University, West Lafayette, Indiana 47907, USA
[3]School of Industrial Engineering, Purdue University, West Lafayette, Indiana 47907, USA
[4]Department of Agricultural and Biological Engineering, Purdue University, West Lafayette, Indiana 47907, USA
[5]School of Electrical and Computer Engineering, Purdue University, West Lafayette, Indiana 47907, USA

[a)]algarner@purdue.edu

ABSTRACT

Gas breakdown is typically driven by Townsend avalanche and predicted mathematically by Paschen's law (PL). Gas breakdown deviates from PL at microscale due to field emission, which depends critically on electrode condition; however, understanding of the impact of initial electrode surface roughness and multiple breakdown events on breakdown voltage is incomplete. This paper assesses the variation of breakdown voltage for a pin-to-plate electrode setup in air at atmospheric pressure for gap distances of $1 \pm 0.5\,\mu$m, $5 \pm 0.5\,\mu$m, and $10 \pm 0.5\,\mu$m with different surface roughnesses. Breakdown voltage generally increases with increasing gap distance and decreasing surface roughness for a single breakdown event; however, the breakdown voltage after ten breakdown events does not depend on initial gap distance. Atomic force microscopy and optical microscopy show that multiple discharges create circular craters on the flat cathode up to $40\,\mu$m deep, with more pronounced craters created at smaller gap sizes and greater cathode surface roughness. The resulting effective gap distances (d_{eff}, the sum of cathode placement distance and crater depth) for subsequent breakdown events are similar to those of the initially larger gap distances. Moreover, d_{eff} becomes sufficiently large to exceed the Meek criterion for streamer formation, indicating a potential for breakdown mechanisms to change from field emission to Townsend avalanche to streamer formation for a single electrode separation distance. The resulting impact of this change in the breakdown mechanism could have significant implications for ensuring consistent microdevice operation.

Published under license by AIP Publishing. https://doi.org/10.1063/1.5085217

I. INTRODUCTION

Miniaturization of electronic components constantly drives innovation in multiple fields, motivating studies of the behavior of electric breakdown and gas discharges at microscale.[1,2] The increased use of microsatellites led to the development of electric micropropulsion to better control them.[3,4] This further motivated the design of chemically reactive, nonreactive, and plasma thrusters, which all suffer from the challenge of applying sufficient energy to the system to alter the propellant without damaging the circuitry used in these micro to nanoscale devices.[5] For microplasma thrusters, the challenge becomes inducing breakdown for propulsion while protecting the devices producing the plasma from excessive damage.[5] A similar challenge arises when developing microplasma systems for biomedical applications.[6]

In electronics, one ideally avoids creating discharges or electrical breakdown. Even for commercializing compact pulsed power systems, one must account for the potential of discharges or arcing that may be detrimental to safe and effective operation. For instance, a recent study developed a flexible, compact pulsed power system for biomedical applications and specifically considered the impact of arcing across electrodes not completely covered by the liquid biological sample on device design.[7] While these

systems typically use gap lengths on the order of millimeters,[7] other applications apply electric pulses to submillimeter gaps,[8] motivating understanding of breakdown in both liquid[9] and gases at these size scales. Electronics designed specifically at these sizes, such as microelectromechanical systems (MEMS), are increasingly used in biotechnology, medicine, and communications.[10] Continuing reduction in the size of MEMS increases the importance of preventing breakdown between their nanofabricated components. Nanoelectromechanical systems (NEMS) are increasingly examined for sensing and scanning[10] with common uses including electronic displays, printers, airbags, and many new MEMS systems. As relevant device sizes transition from microscale to nanoscale, electron emission may shift from field emission to space-charge limited emission,[11,12] motivating additional studies on gas breakdown at a smaller scale. These phenomena also have significant implications in vacuum electronics, where ongoing research in electron sources[13,14] has focused on assessing groups of nanoemitters[15,16] and intentionally modifying device designs to better control field enhancement.[17]

Thus, characterizing gas breakdown and electron emission for microscale and smaller devices is important across application and pressure, motivating studies on the responsible physical phenomena. Gas breakdown is typically driven by Townsend avalanche and predicted by Paschen's law (PL);[18] however, reducing gap sizes to microscale causes field emission to drive breakdown.[2,19,20] This field emission (FE) driven microscale gas breakdown regime is characterized experimentally by the absence of the "Paschen minimum,"[2] or the minimum breakdown voltage V_b typically observed when plotting V_b as a function of the product of gas pressure p and gap distance d, or pd. Instead, V_b exhibits either an extended plateau or a continued decrease with decreasing d at a constant pressure. While the extended plateau occurs near the transition from the PL to the field emission regime, the exact reason why it occurs under certain conditions and not others remains unclear. One contributing factor could be the combination of various aspect ratio nonuniformities on the electrode causing an extended effective Paschen's curve.[21] The individual field emission parameters may also impact the transition from FE to PL, leading to the extended plateau, which can be investigated theoretically. One can mathematically predict the behavior of V_b by coupling field emission with Townsend avalanche[22] and perform a matched asymptotic analysis to derive analytic equations in appropriate limits to demonstrate the transition between the two mechanisms.[23–25] The linear decrease in breakdown voltage for further reductions in gap distance at a constant pressure can be further derived analytically.[25]

One of the critical challenges with predicting this behavior at smaller scales is accurately accounting for the contribution of work function and field enhancement factor,[26] which drive field emission and play the largest role in the sensitivity of predicted V_b at microscale.[27] Since changes in surface roughness can impact the presence of sharp features contributing to field enhancement and localized modifications in electrode structures can modify the work function,[28] experimentally characterizing the impact of surface roughness for microscale gaps is paramount for extending the validity of the theoretical descriptions.[23–25,27] Studies on the impact of surface roughness on emission in vacuum have experimentally considered the formation of field emission sites for unpolished stainless steel electrodes,[29] the impact of electrode microtip formation and destruction on field emission driven vacuum breakdown,[30] and the impact of repeated breakdowns on V_b, current at discharge initiation, field enhancement factor, and the current density as a function of the number of breakdown events.[31]

This study examines the impact of surface roughness and multiple breakdowns on V_b and the electrode surfaces by using a setup comprised of a small tungsten needle placed a few microns from a copper plated sample based on the one used previously to assess atmospheric pressure and field emission driven microdischages.[32] For fixed gap distances of $1 \pm 0.5\,\mu$m, $5 \pm 0.5\,\mu$m, and $10 \pm 0.5\,\mu$m, we measured breakdown voltage and current for a single breakdown event and ten breakdown events, noting the general increase in breakdown voltage for repeated breakdown events, as observed in Ref. 31. This study places these results in the context of electrode modification and surface roughness by using atomic force microscopy (AFM) and light microscopy to show that breakdown events create craters on the cathode with depths ($3–50\,\mu$m) that may be significant compared to the interelectrode gap distance (1, 5, and $10\,\mu$m), contributing to increased V_b. To our knowledge, no microscale experiments have demonstrated the impact of multiple breakdown event induced craters on V_b. Section II outlines the materials and methods used in this study. Section III summarizes the experimental results. We apply microscale gas breakdown theory based on asymptotic analysis to demonstrate the transitions in breakdown mechanisms in Sec. IV. Section V discusses the results and provides concluding remarks.

II. MATERIALS AND METHODS

A. Materials

The setup consists of tungsten dissection needles (Roboz Surgical Instrument Co., RS-6065) mounted into polyethylene to ensure electrical isolation. The copper plates were mounted to polyethylene blocks mounted to a micromanipulator and moved in increments of $1\,\mu$m. Figure 1 shows a schematic of the micromanipulator setup with a fixed pin electrode.

The copper (Fire Mountain Gems, H20–9336FX) was cut into $12.7\,\text{mm}^2$ plates that were then polished to various degrees of surface roughness by using a wet polishing station with 400, 800, and 1200 grit polishing pads (Pace Technologies). After polishing, we soaked the plates in acetone to remove any surface contamination and rinsed them with water to remove any residue. AFM was then conducted to verify the absence of residue or polishing particulate on the surfaces. Table I reports the surface conditions under these initial AFM tests. A wire was soldered onto the back of the copper plate to provide electrical connections. Voltage and current measurements were made using an oscilloscope and two 100:1 voltage probes. One probe was connected across the pin to plate gap to measure the gap voltage and the second across a $1\,\text{M}\Omega$ resistor to determine the current. With the copper plate as the ground (cathode) and the tungsten needle as the "hot" electrode (anode), we used a high voltage supply (Stanford Research System, PS365, 10 kV) to apply DC voltage until discharge formation.

Published under license by AIP Publishing.

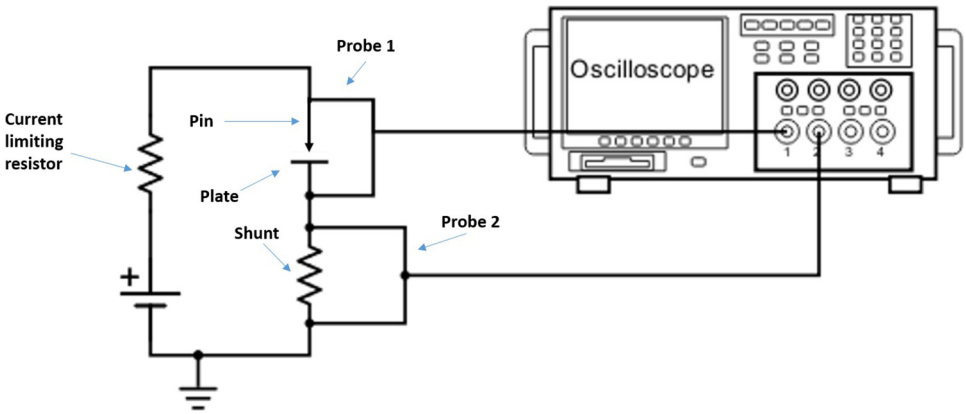

FIG. 1. Schematic of the experimental setup with a pin to plate configuration to test samples.

B. Methods

We divided each copper plate into sections for single breakdown event testing, ten breakdown event testing, and sample handling. We tested cathodes polished with each grit in triplicate for statistical purposes. We set the gap distance by applying 35 V to create a bias and using the micromanipulator to move the plate until it softly contacted the needle to create a "short" in the circuit before withdrawing the plate to the desired gap distance. This method was previously used to calibrate needle electrode distance with no effect on the surface.[32] To determine whether the contact phase of the setup damaged the surface, we used the micromanipulator to force a needle electrode into the surface. AFM was used to verify that no significant change to the electrode surface was measurable. We considered gap distances of $1 \pm 0.5\,\mu$m, $5 \pm 0.5\,\mu$m, and $10 \pm 0.5\,\mu$m between the needle and the copper plate. Voltage was ramped at approximately 3 V/s from 100 V to breakdown, where an oscilloscope recorded the breakdown voltage and current waveforms. We removed the voltage immediately following the oscilloscope trigger to prevent further breakdown events. Since no current was present before breakdown, there was no voltage across the 1 MΩ resistor prior to breakdown, so this voltage served as an indication of breakdown. We collected voltage and current waveforms for each breakdown event to compare breakdown voltage across events. Breakdown for these tests was defined as the movement of electrons across the gap, creating a sustained dielectric breakdown of the gas. The current was limited using a ballast resistor to prevent damage to the anode and prevent large currents across the gap that would damage the tip. We observed no damage to the tungsten tips. The discharge event was measured by a shunt resistor that allowed us to monitor the current. When the current across the gap was detected by the oscilloscope, we immediately turned off the power supply to ensure that we only created a single breakdown event at a time. For the ten breakdown experiments, we waited 1 min after each breakdown event before repeating. The relative humidity varied from 38% to 50% during the course of experiments.

We used atomic force microscopy (AFM) to quantify the change in surface roughness by measuring the average height of surface features before and after the breakdown events. Some breakdown induced surface features were too deep for AFM analysis and were estimated by altering the depth of field of an optical microscope to observe when the bottom of the feature was in focus compared to the surface.

TABLE I. Average surface features before breakdown tests.

Grit	Number of samples	Peak to peak average (μm)	Standard deviation (μm)	RMS (nm)
400	9	1.47	1.08	535.22
800	9	0.26	0.18	65.99
1200	9	0.24	0.23	39.48

III. RESULTS

A. Cathode surface changes

Figure 2 shows the representative AFM data for the 800 grit polished cathode prior to breakdown experiments using a 5 μm gap. The optical images of the surface, such as Fig. 2(a), show the general roughness of the surface. Figure 2(b) shows the contour map of the 800 grit sample with a maximum surface height of 200 nm and a crater depth of 200 nm. Figure 2(c) shows the AFM tip deflection that measures the surface feature height. This was repeated for each sample to characterize the average surface features before the breakdown experiments. Table I presents the initial average surface feature height for the samples before breakdown events along the red dashed line in Fig. 2(b). The data in Table I were taken by averaging all of the peak to peak and RMS values for each grit.

The breakdown events created small circular ablations on the samples at the test site. Figure 3 shows an optical image of an example ablated feature for a cathode polished using 800 grit exposed to ten breakdown events at a 5 μm gap distance. The ablation depth ranged from 3 to 50 μm and is reported in Table II for all samples containing them. The depth was so great that the samples could not be measured using AFM to quantify the surfaces without damaging the AFM tips. These results indicate that breakdown can cause significant surface modification, ablating material from a localized spot. Furthermore, the ablation depth is greatest for the cathodes with the largest average surface height (400 grit polished cathodes), which would be anticipated to have the highest

Published under license by AIP Publishing.

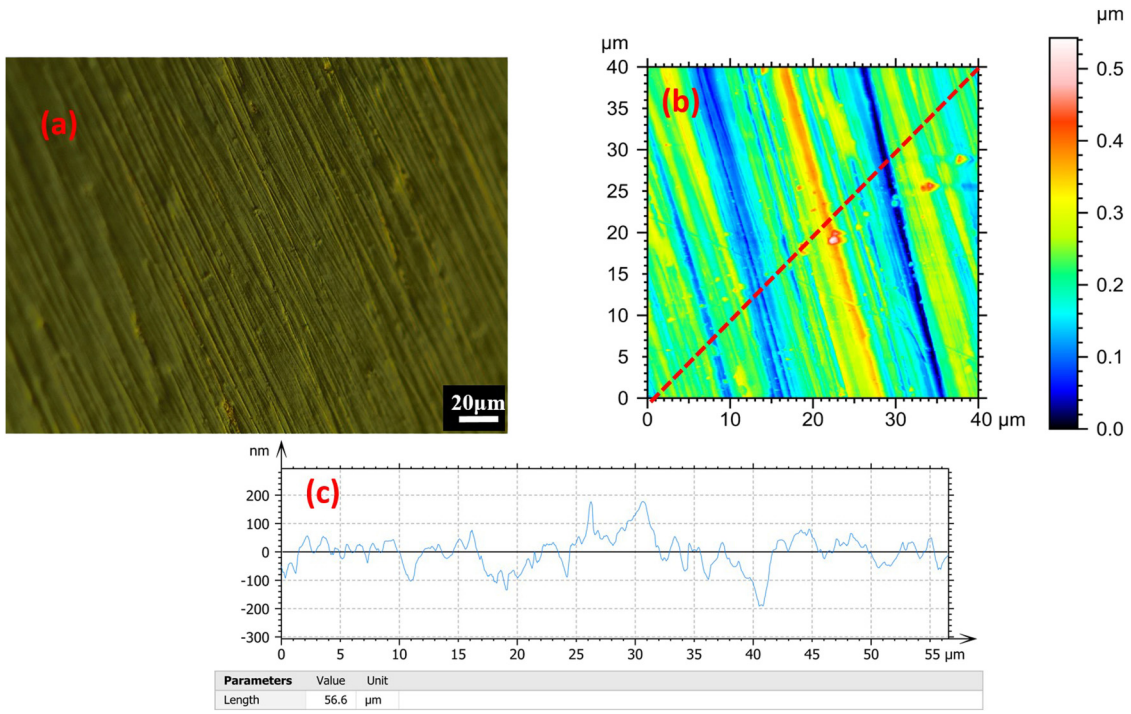

FIG. 2. Atomic force microscopy (AFM) measurements of the 800 grit cathode prior to experiments showing the average surface features (a) Optical image of the surface visually showing the surface roughness. (b) Contour mapping of surface height along the surface. (c) AFM arm deflection showing height and depth of the surface features.

field enhancement and, thus, be more susceptible to field emission driven breakdown. This suggests that the concentration of the discharges at the locations of higher surface height for the cathodes polished with 400 grit causes greater cathode damage compared to the 800 and 1200 grit samples, whose surface features are less sharp and will cause less field enhancement.

To determine whether the contact phase of the setup damaged the surface, we used the micromanipulator to force a needle electrode into the surface. AFM was used to verify that no significant change to the electrode surface was measurable. The resulting absence of a circular mark indicated that the breakdown events, and not needle placement, damaged the surface. The absence of these marks on some samples following breakdown indicated that slight variations in surface polishing, which could influence the initial presence of surface structures, could sufficiently alter discharge path and subsequent surface ablation.

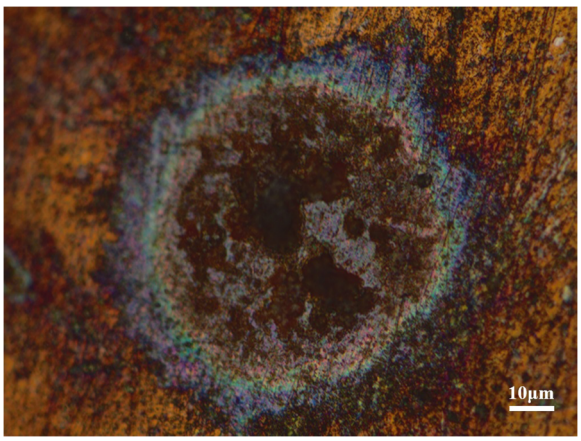

FIG. 3. Observed ablated region on the cathode after ten breakdown events for a 5 μm gap with the cathode polished using 800 grit, demonstrating the crater formed in the surface.

TABLE II. Depth of the observed craters at the breakdown voltage for the cathodes polished at each grit where measurable ablation occurred.

Grit (gap distance)	Depth (μm)	Grit (gap distance)	Depth (μm)	Grit (gap distance)	Depth (μm)
400 (10 μm)	9.7	800 (5 μm)	6.2	1200 (1 μm)	12.1
400 (10 μm)	6	800 (5 μm)	7.4	1200 (1 μm)	3.5
400 (10 μm)	13.5	800 (5 μm)	12.4	1200 (10 μm)	4.8
400 (5 μm)	41.2	800 (5 μm)	5.3	1200 (10 μm)	5.4
400 (5 μm)	19.6	800 (5 μm)	5.2		
400 (1 μm)	42.5				

Published under license by AIP Publishing.

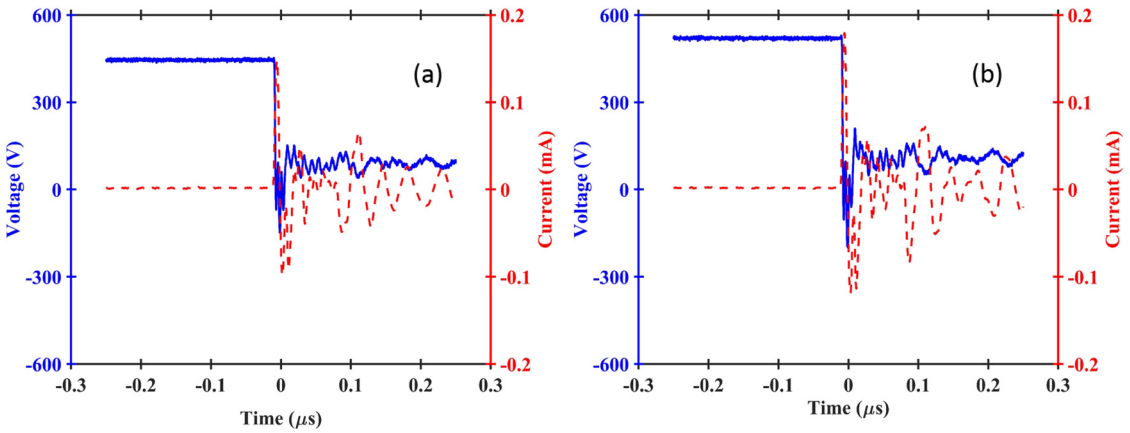

FIG. 4. Representative voltage (solid) and current (dashed) waveforms for a $5 \pm 0.5\,\mu$m gap with the cathode polished using 800 grit for (a) a single breakdown event and (b) the tenth breakdown event. All breakdown events exhibited similar characteristics.

B. Changes in breakdown voltage

Figure 4 shows a representative waveform for a single breakdown event and the tenth breakdown event for a $5 \pm 0.5\,\mu$m gap distance with the cathode polished using 800 grit. The voltage remains relatively constant until breakdown occurs, as expected for an applied DC voltage. The breakdown voltage following the tenth event exceeded that for a single event, as shown in Fig. 6. In this case, the first breakdown event occurred at 434.85 V, while the tenth breakdown occurred at 523.25 V.

Figures 5–7 report the individual replicates for breakdown voltage as a function of the number of breakdown events for a 1, 5, and $10\,\mu$m gap with cathodes polished using 400, 800, and 1200 grit disks. Note that we did not achieve three repetitions for a few of the ten breakdown event cases due to either reaching high voltages for larger gap distances or slight sensitivity to micromanipulator position for smaller gap distances. Figure 8 reports the average values for a given grit. Generally, breakdown voltage increases with subsequent breakdown events, although this difference is not monotonic and noticeable variation occurs between samples.

Because the craters make noting distinct differences challenging, we ran a general linear model analysis of variance (ANOVA) with stepwise backward elimination to identify the statistically significant difference in means based on voltage as the response for each breakdown event (Minitab 18 software). Anderson–Darling normality tests showed no significance (p-values >0.05), indicating normal distribution of residuals, except for the ninth pulse, which likely arises due to some outliers in our experimental dataset when reaching the limit of the micromanipulator travel tolerances. The ANOVA was followed by a Tukey pairwise comparison test at the 95% confidence level and adjusted p-values are reported due to the need for multiple comparisons. The grit did not exhibit any significance for any of the tests. The gap showed significant differences

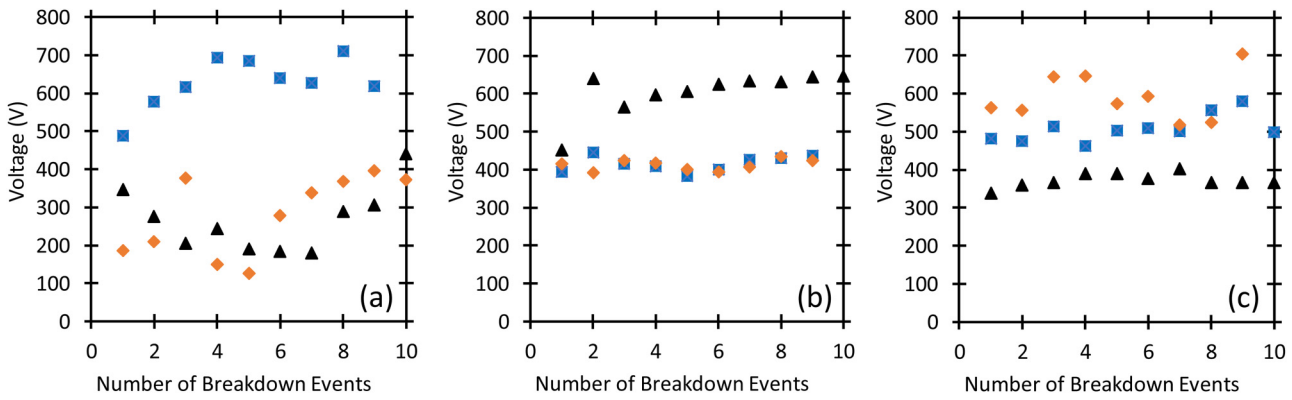

FIG. 5. Breakdown voltage as a function of number of breakdown events for three individual trials for (a) 400 grit, (b) 800 grit, and (c) 1200 grit samples at a $1\,\mu$m gap distance.

Published under license by AIP Publishing.

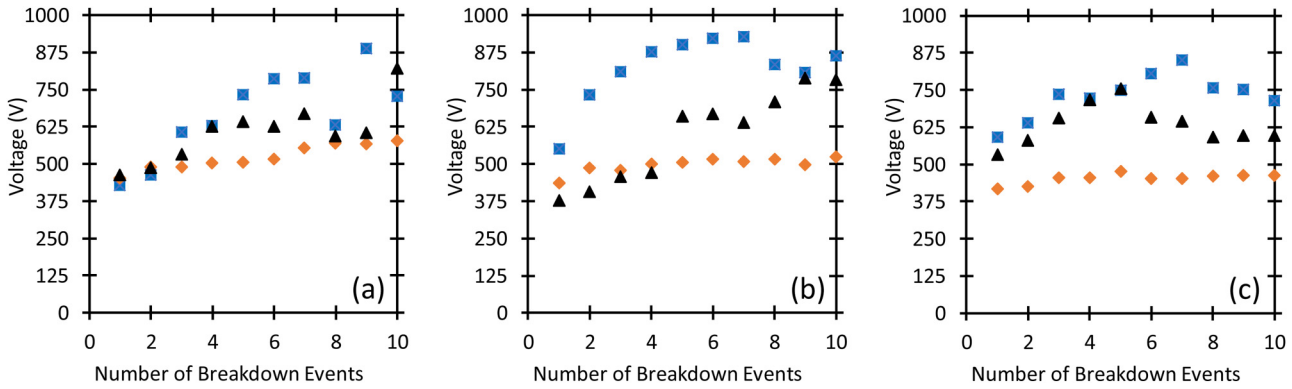

FIG. 6. Breakdown voltage as a function of number of breakdown events for three individual trials for (a) 400 grit, (b) 800 grit, and (c) 1200 grit samples at a 5 μm gap distance.

in means for voltage after at least five breakdown events ($p < 0.05$). Table III summarizes the adjusted p-values from the Tukey tests for significance. Breakdown voltages for a 1 μm gap after at least five breakdown events differ statistically significantly from either the 5 μm or 10 μm gaps, while the breakdown voltages following the fifth breakdown event for the 5 μm and 10 μm gaps do not exhibit any statistically significant difference.

This behavior arises because the breakdown events alter the electrode surface, which also contributes to the increased variation after multiple events. First, each breakdown ablates the sharp-tipped features that contribute to field enhancement, meaning that the applied voltage (and, thus, the electric field) for subsequent breakdown events must exceed the breakdown voltage for the initial event. The breakdown events additionally create craters on the surface that increase the effective gap distance, as shown by comparing Tables I and II, further increasing the applied voltage to achieve the electric field necessary for breakdown. Thus, we anticipate that the combination of these phenomena will cause a general increase in breakdown voltage for subsequent breakdown events. This trend may not necessarily be monotonic since changes to the electrode surface structure (both electrode depth and field enhancement factor) may vary from event to event and across samples.

This suggests that the change in the effective gap distance induced by crater formation plays a dominant role in breakdown voltage for multiple events. Table IV shows that the crater depth is highest for the smallest gap distances, where field emission tends to drive breakdown,[2,25–27] and for the cathode (400 grit) with the sharpest surface features, which would initially provide greater field enhancement to further drive field emission. Thus, we anticipate that the discharges under these conditions would focus on the sharp emitters during repeated breakdowns, resulting in greater cathode damage characterized by larger craters. These larger craters would increase the effective gap distance, which also corresponds to a higher field enhancement factor in the combined field emission/Townsend avalanche regime since field enhancement increases with increasing gap distance in this regime.[32] Eventually,

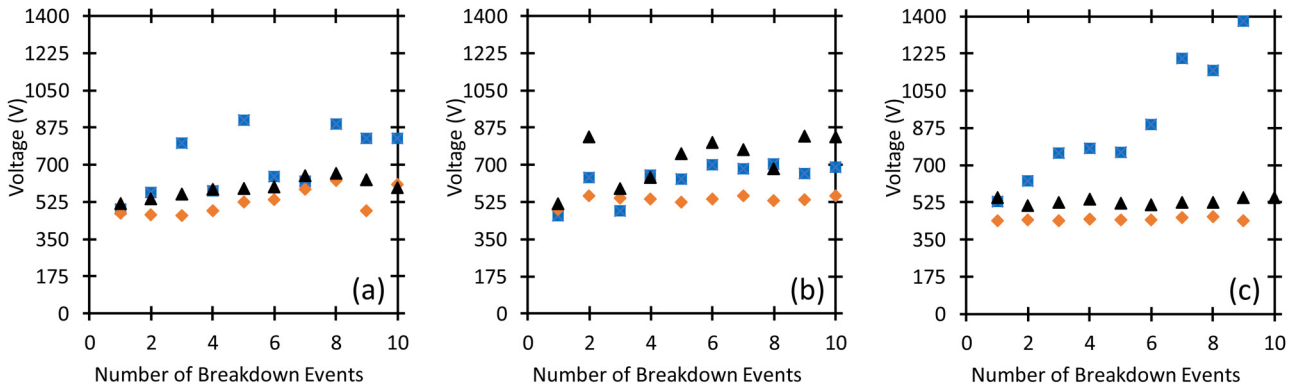

FIG. 7. Breakdown voltage as a function of number of breakdown events for three individual trials for (a) 400 grit, (b) 800 grit, and (c) 1200 grit polished cathodes at a 10 μm gap distance.

Published under license by AIP Publishing.

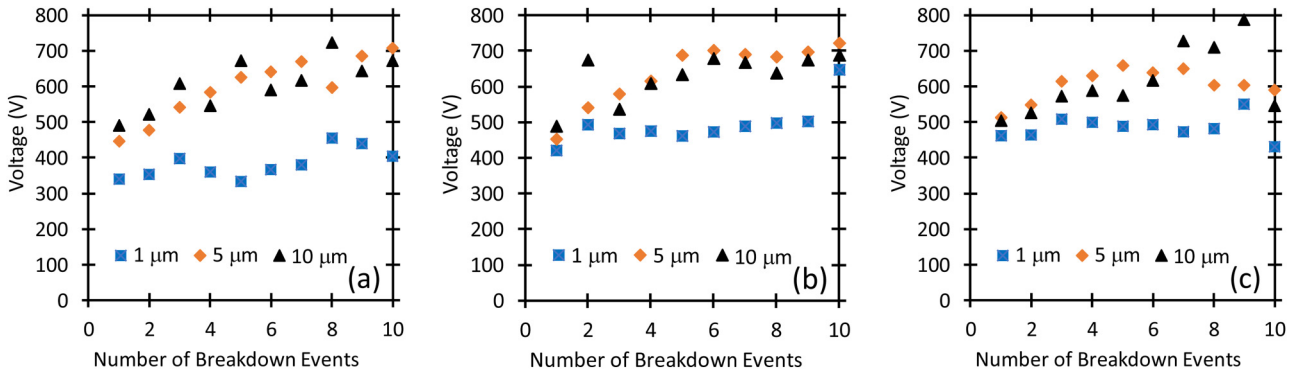

FIG. 8. Average breakdown voltage as a function of number of breakdown events for (a) 400 grit, (b) 800 grit, and (c) 1200 grit for three trials each.

these larger effective gap distances could also lead to a transition in the breakdown mechanism from field emission to Townsend avalanche. Section IV applies an asymptotic theory for microscale gas breakdown to confirm this hypothesis and quantify the contributions of the phenomena involved.

Figure 8 shows larger gap sizes did not always result in higher breakdown voltage, as one would intuitively expect. The variation in breakdown voltage is likely due to the crater formation, which leads to a larger effective gap. Table IV presents the average crater depths for the conditions where craters occurred. Since this experiment considered conditions only after either a single breakdown event or ten breakdown events, we did not record information on crater formation for intermediate conditions (i.e., the exact number of events when crater formation occurred).

IV. THEORETICAL ASSESSMENT

Table IV summarizes the average crater depth for various grits and initial gap distances, along with the average breakdown voltage following the first and tenth breakdown events. Strictly speaking, we would need the crater depth after the ninth breakdown event to calculate the average breakdown voltage after the tenth event; however, the data indicate relatively slight variation between the breakdown voltage for the ninth and tenth events, so we use this crater depth for these calculations. Applying an "effective gap distance" that combines the initial gap distance with the crater depth allows us to assess the transition in breakdown mechanisms with crater formation, analogous to our previous theoretical studies.[23–25,27] It is critical to point out that applying the theory to the "raw" data from Figs. 5–8 would lead to large variations in the fitting parameters; however, accounting for the crater depth using Table II dramatically reduces the relative error of the gap distances (particularly compared to the raw data), enabling the application of the theory.[27] While variation clearly remains (which motivated the study from Ref. [27]), we apply the theory here to clearly emphasize the behavior of breakdown voltage as a function of gap distance and the transitions in breakdown regime that we have observed elsewhere.[25]

We start from our previously derived universal gas breakdown model,[24] given by

$$\frac{\exp[\bar{\phi}^{3/2}/(\beta\bar{E})]}{\beta\bar{\phi}^{1/2}\exp(\bar{\phi}^{-1/2})}\sqrt{\frac{\bar{T}\bar{E}}{\bar{p}\bar{d}_{eff}^{2}}\frac{\{1-\gamma_{SE}[\exp(\bar{\alpha}\bar{d}_{eff})-1]\}}{\exp(\bar{\alpha}\bar{d}_{eff})-1}}=\exp(1)(1+2\bar{E}), \tag{1}$$

TABLE III. Adjusted *p*-values from Tukey tests comparing breakdown voltage for 5 μm and 1 μm gaps, 10 μm and 1 μm gaps, and 10 μm and 5 μm gaps for the fifth through tenth breakdown events. Generally, breakdown events after the fifth event yield a statistically significant breakdown voltage between the 1 μm gap and the other gap distance, while no statistically significant difference arises between the 5 μm and the 10 μm gaps.

Breakdown event	Difference between 5 μm and 1 μm	Difference between 10 μm and 1 μm	Difference between 10 μm and 5 μm
5	0.015[a]	0.038[a]	0.914
6	0.017[a]	0.044[a]	0.900
7	0.036[a]	0.035[a]	1.000
8	0.141	0.026[a]	0.693
10	0.002[a]	0.005[a]	0.988

[a]Conditions undergoing a statistically significant change.

TABLE IV. Average crater depth and breakdown voltage after the tenth breakdown event.

Grit	Starting gap distance (μm)	Average crater depth (μm)	Average breakdown voltage for 1st event (V)	Average breakdown voltage for 10th event (V)
400	1	42.5	339	405
400	5	30.4	446	707
400	10	9.73	491	672
800	5	7.3	454	723
1200	1	7.8	462	432
1200	10	5.1	504	545

Published under license by AIP Publishing.

TABLE V. Summary of parameters used in the theoretical analysis.

Parameter	Name	Value	Unit
ϕ	Work function	4.7	eV
ϕ_*	Work function scale	96.81	eV
d	Gap distance	Variable	m
L	Gap distance scale	3.92×10^{-12}	m
p	Pressure	760	Torr
p_*	Pressure scale	1.70×10^{8}	Torr
E	Breakdown electric field	Variable	V/m
E_*	Breakdown electric field scale	6.20×10^{12}	V/m
V	Breakdown voltage	Variable	V
V_*	Breakdown voltage scale	24.3	V
T	Temperature	300	K
T_*	Temperature scale	7976	K
β	Field enhancement factor	Variable	N/A
γ_{SE}	Secondary emission coefficient	10^{-5}	N/A

where $\bar{E} = E/E_*$ is the dimensionless breakdown field, $\bar{d}_{eff} = \bar{d} + \bar{\delta} = (d+\delta)/L$ is the effective dimensionless gap distance with $\bar{d}$ the dimensionless electrode gap distance and $\bar{\delta}$ the dimensionless crater depth, $\bar{\phi} = \phi/\phi_*$ is the dimensionless work function, $\bar{p} = p/p_*$ is the dimensionless pressure, $\bar{T} = T/T_*$ is the dimensionless gas temperature, and Table V defines all other parameters and provides typical values.

We numerically solve (1) for $\bar{E}$ and apply $V = \bar{E}\bar{d}_{eff}E_*L$ to obtain the breakdown voltage in volts using β as a fitting parameter. Furthermore, since the product of the ionization coefficient α and d exceeds unity (specifically, $1.1 < \bar{\alpha}\bar{d}_{eff} = \bar{p}\bar{d}_{eff}\exp(\bar{p}\bar{d}_{eff}\exp(-1)) < 50$, where $\bar{\alpha} = \alpha L$), we apply the analytic equation for breakdown voltage for $\bar{\alpha}\bar{d} \gg 1$, given in Ref. 24,

$$V = (E_*L\bar{d}_{eff}/\Lambda_2)[-\Delta_2 - (\Delta_2^2 - 2\Lambda_2\bar{\phi}^{3/2}/\beta)^{1/2}], \tag{2}$$

where $\Delta_2 = -[\bar{\mu} + \bar{\nu}]$ and $\bar{\mu} = \ln(\Lambda_2)/2 + \ln(\beta\bar{\phi}^{1/2}) + \bar{\phi}^{-1/2} + 3/2$ and $\bar{\nu} = \ln\{\exp[\bar{p}\bar{d}_{eff}\exp(-1)] - 1\} - \ln\{1 - \gamma_{SE}[\exp(\bar{p}\bar{d}_{eff}\exp(-1))]\} - \ln[\bar{T}\bar{p}^{-1}\bar{d}_{eff}^{-2}]/2$ represent the field emission and Townsend contributions, respectively, and $\Lambda_2 = 10^{-5}$ is a fitting parameter. Figure 9 shows the experimental results (correcting for effective gap distance, which means that many of these points are individual points from Table II), the calculations from (1) and (2), and the values of $\bar{\alpha}\bar{d}_{eff}$ (note that $\bar{\alpha}\bar{d}_{eff} = \alpha d_{eff}$ since both quantities are scaled by L). Note that several d_{eff} have multiple data points due to crater formation changing d_{eff} under various conditions. From Meek's criterion,[33] $\bar{\alpha}\bar{d}_{eff} \approx 18$ corresponds to the transition to streamer formation, making (1) and (2) no longer valid [in fact, (2) is unsolvable for these points]. Although we have addressed this limitation to this theory in previous studies,[23–25] this experimental condition is unique, in that we start in the field emission regime and then transition to the Townsend and streamer regimes without changing the physical gap distance. Current theory does not address the transition to streamer discharge at microscale, so we note the potential transition in the current study. The results of (1) and (2) differ by ~10% except for the two largest gap distances where $\bar{\alpha}\bar{d}_{eff} > 18$ and (2) cannot be solved.

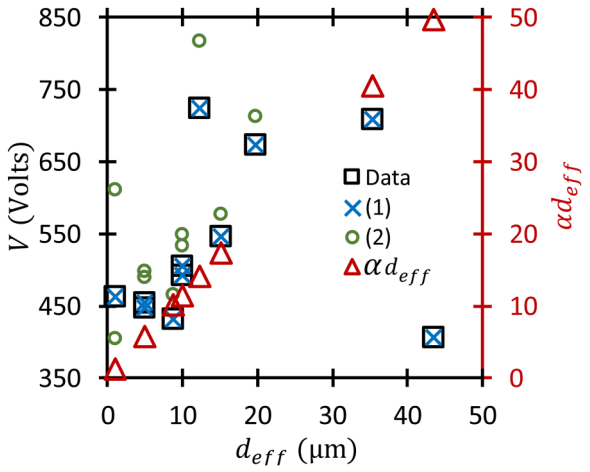

FIG. 9. Average breakdown voltage, V, as a function of effective gap distance, $d_{eff} = d + \delta$, where d is the anode–cathode gap and δ is the breakdown induced crater depth, compared to numerical results from (1) and analytic results from (2). The product of the ionization coefficient and effective gap distance, αd_{eff}, is displayed on the secondary vertical axis as a function of d_{eff}. The largest two gap distance points have $\alpha d_{eff} \gg 18$, which exceeds Meek's criterion for streamer formation.

Figure 10(a) shows β for fitting the model to experimental data. Interestingly, β varies linearly with d_{eff} until the largest gap distances, excluding the outlier at $d_{eff} \approx 12\,\mu$m. At the largest gaps, β becomes approximately constant. This behavior is similar to our previous application of this theory to experimental results for single breakdown events at microscale, where β increased linearly until Townsend avalanche began to dominate.[25] Furthermore, the transition from linear to constant β occurs approximately when $\bar{\mu} = \bar{\nu}$, or when breakdown begins to transition from field emission to the traditional Paschen law.[18,26,27,34] Figure 10(b) shows that $\alpha d_{eff} \approx 10$ at this transition.

Upon transition to Paschen's law, the experimental data and numerical results from (1) agree well with the universal Paschen's law (UPL),[24] given by

$$V = \frac{(\bar{p}\bar{d}_{eff})}{\ln(\bar{p}\bar{d}_{eff}) - \ln[\ln(1 + \gamma_{SE}^{-1})]}(E_*L). \tag{3}$$

Figure 11 shows the experimental results, the numerical results from (1), and the results of (3) using $\gamma_{SE} = 1.5 \times 10^{-3}$, which we selected based on previous studies[24,25,27] and agreement with the experimental data. The calculations from (1) for the asymptotic solution match (3) for the UPL when $\alpha d_{eff} \approx 10$, corresponding to the transition from the combined field emission and Townsend regime to the traditional Paschen's law, and deviate once αd_{eff} becomes sufficiently large for streamer formation. Alternatively, noting that the transition to Paschen's law occurs when $\alpha d_{eff} \approx 10$, we can calculate γ_{SE} to match the experimental results by solving (3) to obtain $\gamma_{SE} = \{\exp[\bar{p}\bar{d}_{eff}\exp(-\bar{p}\bar{d}_{eff}/\bar{V})] - 1\}^{-1}$. Future work

Published under license by AIP Publishing.

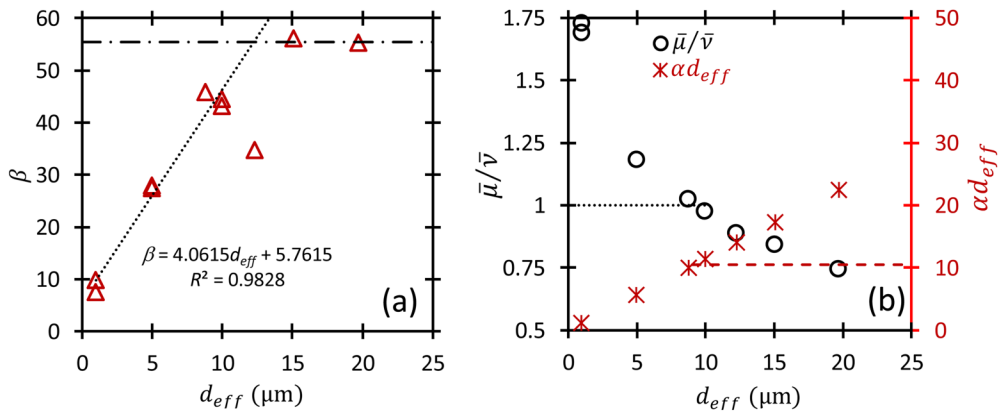

FIG. 10. (a) Field enhancement factor, β, as a function of effective gap distance, $d_{eff} = d + \delta$, where d is the gap distance and δ is the crater depth, showing that β is approximately linear until the larger gap distances corresponding to the transition to Townsend avalanche, where it becomes constant. (b) The ratio of the field emission component to the Townsend component, $\bar{\mu}/\bar{v}$, as a function of d_{eff}, demonstrating that field emission effects govern breakdown until $d_{eff} \approx 10\,\mu$m, which corresponds to $\alpha d_{eff} \approx 10$. This point coincides with the transition of β from linear to constant in (a), indicating the transition to the traditional Paschen's law.

will aim to better characterize γ_{SE} and further assess streamer formation and behavior.

Finally, we theoretically assess the impact of crater formation on breakdown voltage. Figure 12 summarizes the six sets of data, showing αd_{eff} after one and ten breakdown events. Notably, the data from the samples with initial gap distances of 1 and 5 μm had $\alpha d_{eff} < 10$ after the first breakdown event, but transitioned to $\alpha d_{eff} > 10$ after the tenth breakdown event, indicating that crater formation alone can push the breakdown mechanism into the Townsend regime even if the anode–cathode gap remains unchanged. This could have significant implications on device design, where many breakdown events are expected to occur and breakdown voltage is expected to remain constant. Moreover, this suggests that eventually, subsequent breakdown events will not increase crater depth much since one transitions to the Townsend regime, where field enhancement diminishes, reducing the localization of breakdown that occurs at smaller gaps in the field emission regime. This suggests that most sensitivity to the influence of surface effects in breakdown occurs when operating in the field emission regime with rough cathodes, where the higher electric fields lead to greater crater formation and noticeable changes in breakdown voltage and electrode conditions.

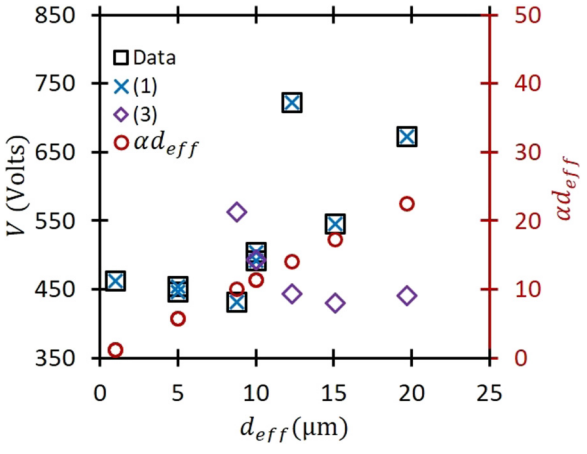

FIG. 11. Breakdown voltage, V, as a function of effective gap distance, $d_{eff} = d + \delta$, where d is the gap distance and δ is the crater depth, from the experimental data, the numerical results of (1), and the analytic results of (3) assuming $\gamma_{SE} = 1.5 \times 10^{-3}$. The product of the ionization coefficient and effective gap distance, αd_{eff}, is shown on the secondary vertical axis. The transition to Paschen's law (PL) occurs for $\alpha d_{eff} \approx 10$. PL predicts breakdown until it becomes driven by streamer formation when $\alpha d_{eff} > 18$.

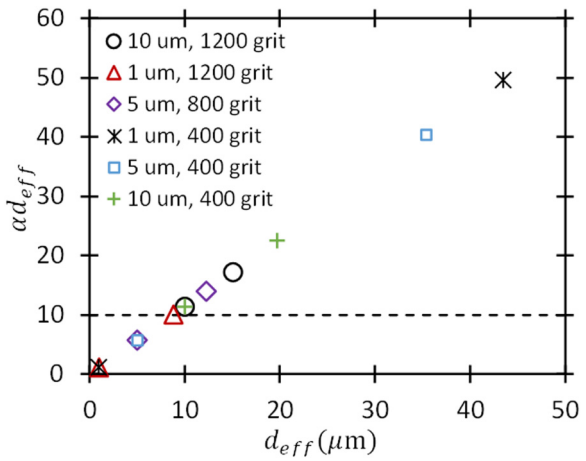

FIG. 12. The product of the ionization coefficient and effective gap distance, αd_{eff}, as a function of the effective gap distance gap distance, $d_{eff} = d + \delta$, where d is the gap distance and δ is the crater depth. Each pair of symbols shows the αd_{eff} value after the first and tenth breakdown events, showing that crater formation can push breakdown behavior past the $\alpha d_{eff} \approx 10$ criterion for transition to Paschen's law.

Published under license by AIP Publishing.

V. CONCLUSION

These results show the dependence of breakdown voltage on repeated breakdown events for a pin-to-plate configuration at microscale gaps and atmospheric pressure. With a polished copper plate as the cathode and a tungsten dissection needle as the anode, we measured the breakdown voltage for 1, 5, and $10 \pm 0.5\,\mu$m gaps. We polished the cathodes using 400, 800, and 1200 grit papers with a wet polishing machine to vary the surface roughness. Figures 5–7 show that the change in breakdown voltage due to surface roughness for a fixed gap distance or due to gap distance for a fixed surface roughness was not statistically significant. The major change in behavior involved the variation in breakdown voltage due to cathode crater formation. AFM and optical imaging before and after the breakdown events showed that the cathodes changed from having average surface feature heights ranging from 0.24 to $1.47\,\mu$m before the events to containing small ablated regions with crater depths ranging from 3 to $50\,\mu$m (cf. Table II). The combination of initial surface feature height and the ablation/melting of surface material changed the effective gap distance of the system. Cathode crater formation drove the changes by increasing the effective gap distance, which increased breakdown voltage for multiple breakdown events. We observed similar breakdown voltages for similar effective gap distances independent of the interelectrode spacing. Applying a matched asymptotic analysis to the experimental results demonstrated that the breakdown voltage was a function of the effective gap distance and that the transition from field emission to Townsend avalanche occurred at effective gap distances equivalent to the gap distances observed for single breakdown studies.[24,25] Moreover, β varied linearly with gap distance in the field emission regime before becoming constant at the transition to the Townsend avalanche, as observed for single breakdown studies.[25] Interestingly, we observed a change in dominant breakdown mechanism from field emission to Townsend avalanche to streamer discharge at a single interelectrode gap distance due to crater formation. Thus, for microscale devices, changes in electrode surface can play a major role in breakdown voltage for multiple uses, particularly for rough surfaces where field emission dominates, leading to concentration of discharge formation at the emission sites that creates large craters.

While the current study focused on the breakdown voltage and surface structure, predominantly cathode feature height or depth, sensitivity analysis of the breakdown theory indicates that microscale gas breakdown voltage also depends strongly on work function.[27] Future studies will extend the analysis to assess changes in work function with repeated breakdown events to ascertain the relative contribution on gas breakdown, particularly when uncertainty in work function and field enhancement dominate the sensitivity of breakdown voltage predictions for gap distances below $10\,\mu$m.[27] Although mean surface roughness did not impact the breakdown voltage, it did lead to concentration of the discharge at emission sites that impacted subsequent breakdown events; however, this study did not consider the impact of a single, controllable sharp-tipped emitter on breakdown voltage. Future studies will, thus, further investigate the impact of controllable aspect ratio[17] as a function of gap distance and pressure on gas breakdown and current density to additionally characterize transitions between electron emission mechanisms[10,14] and breakdown phenomena.

ACKNOWLEDGMENTS

We gratefully acknowledge funding from the Office of Naval Research (ONR) (Grant No. N00014–17-1–2702). A.M.L. also gratefully acknowledges funding from a graduate scholarship from the Directed Energy Professional Society. We also thank Robert Bean for allowing the use of his facilities and equipment for performing many of the experiments and Sean Dinn for valuable discussions on applying statistical analyses to our data.

REFERENCES

[1]K. H. Schoenbach and K. Becker, Eur. Phys. J. D **70**, 29 (2016).
[2]D. B. Go and A. Venkattraman, J. Phys. D Appl. Phys. **47**, 503001 (2014).
[3]W. P. Wright and P. Ferrer, Prog. Aerosp. Sci. **74**, 48 (2015).
[4]M. Martinez-Sanchez and J. E. Pollard, J. Propuls. Power **14**, 688 (1998).
[5]C. Charles, J. Phys. D Appl. Phys. **42**, 163001 (2009).
[6]F. Iza, G. J. Kim, S. M. Lee, J. K. Lee, J. L. Walsh, Y. T. Zhang, and M. G. Kong, Plasma Process. Polym. **5**, 322 (2008).
[7]A. L. Garner, A. Caiafa, Y. Jiang, S. Klopman, C. Morton, A. S. Torres, A. M. Loveless, and V. B. Neculaes, PLoS One **12**, e0181214 (2017).
[8]J. F. Kolb, S. Kono, and K. H. Schoenbach, Bioelectromagnetics **27**, 172 (2006).
[9]K. H. Schoenbach, J. Cooper, A. Garner, B. Goan, R. P. Joshi, J. Kolb, S. Katsuki, S. Kono, M. Laroussi, F. Leipold, X. Lu, C. Mallot, J. Quian, and S. Xiao, AIP Conf. Proc. **650** 111–114 (2002).
[10]R. Bogue, Sens. Rev. **27**, 7 (2007).
[11]Y. Y. Lau, Y. Liu, and R. K. Parker, Phys. Plasmas **1**, 2082 (1994).
[12]A. M. Darr, A. M. Loveless, and A. L. Garner, Appl. Phys. Lett. **114**, 014103 (2019).
[13]K. L. Jensen, IEEE Trans. Plasma Sci. **46**, 1881 (2018).
[14]P. Zhang, Á Valfells, L. K. Ang, J. W. Luginsland, and Y. Y. Lau, Appl. Phys. Rev. **4**, 11304 (2017).
[15]W. W. Tang, D. A. Shiffler, J. R. Harris, K. L. Jensen, K. Golby, M. LaCour, and T. Knowles, AIP Adv. **6**, 95007 (2016).
[16]J. R. Harris, K. L. Jensen, and D. A. Shiffler, AIP Adv. **5**, 87182 (2015).
[17]J. Lin, P. Y. Wong, P. Yang, Y. Y. Lau, W. Tang, and P. Zhang, J. Appl. Phys. **121**, 244301 (2017).
[18]F. Paschen, Ann. Phys. **273**, 69 (1889).
[19]Z. L. Petrović, N. Škoro, D. Marić, C. M. O. Mahony, P. D. Maguire, M. Radmilović-Rađenović, and G. Malović, J. Phys. D Appl. Phys. **41**, 194002 (2008).
[20]M. Radmilović-Radjenović and B. Radjenović, Plasma Sources Sci. Technol. **17**, 24005 (2008).
[21]Y. Fu, P. Zhang, and J. P. Verboncoeur, Appl. Phys. Lett. **112**, 254102 (2018).
[22]A. Venkattraman and A. A. Alexeenko, Phys. Plasmas **19**, 123515 (2012).
[23]A. M. Loveless and A. L. Garner, Appl. Phys. Lett. **108**, 234103 (2016).
[24]A. M. Loveless and A. L. Garner, Phys. Plasmas **24**, 113522 (2017).
[25]G. Meng, X. Gao, A. M. Loveless, C. Dong, D. Zhang, K. Wang, B. Zhu, Y. Cheng, and A. L. Garner, Phys. Plasmas **25**, 82116 (2018).
[26]R. H. Fowler and L. Nordheim, Proc. R. Soc. A Math. Phys. Eng. Sci. **119**, 173 (1928).
[27]S. D. Dynako, A. M. Loveless, and A. L. Garner, Phys. Plasmas **25**, 103505 (2018).
[28]W. Li and D. Y. Li, J. Chem. Phys. **122**, 64708 (2005).
[29]B. M. Cox and W. T. Williams, J. Phys. D Appl. Phys. **10**, L5 (1977).
[30]G. N. Fursey, IEEE Trans. Electr. Insul. **EI-20**, 659 (1985).
[31]D. W. Williams and W. T. Williams, J. Phys. D **7**, 1173 (1974).
[32]M. A. Bilici, J. R. Haase, C. R. Boyle, D. B. Go, and R. M. Sankaran, J. Appl. Phys. **119**, 223301 (2016).
[33]L. B. Loeb and J. M. Meek, *Mechanism of Electric Spark* (Stanford University Press, Stanford, CA, 1941).
[34]A. M. Loveless and A. L. Garner, IEEE Trans. Plasma Sci. **45**, 574 (2017).

Published under license by AIP Publishing.